JOURNAL OF THEORETICAL AND APPLIED MECHANICS
61, 3, pp. 559-571, Warsaw 2023
https://doi.org/10.15632/jtam-pl/168072

BUCKLING AND VIBRATION OF POROUS SIGMOID FUNCTIONALLY GRADED CONICAL SHELLS

Xiaolin Huang, Jiaheng Wang, Nengguo Wei, Chengzhe Wang, Bin Ma
School of Architecture and Transportation Engineering, Guilin University of Electronic Technology, Guilin, China
corresponding author Bin Ma, e-mail: 780227067@qq.com

In this study, the buckling and vibration of a sigmoid functionally graded material (S-FGM) shells are investigated. Two types of porosity distributions, even and uneven, are taken into account. The material properties are estimated by a new modified rule of mixture. In the framework of the classic thin shell theory, the governing equations are derived and Galerkin's integrate technique is employed to compute the critical load and natural frequency of porous S-FGM shells. The influence of pores, ceramic mass fraction and materials power index are discussed in detail.

Keywords: functionally graded materials, pore, conical shell, buckling, vibration

1. Introduction

In the past two decades, many studies have been devoted to the buckling and vibration of functionally graded conical shells (Sofiyev, 2019). Sofiyev and his coauthors have made a prominent contribution to those studies. By using the Donnell shell theory and the Galerkin method, they obtained a series of analytical solutions to buckling loads and lowest natural frequencies of non-homogeneous orthotropic conical shells (Sofiyev *et al.*, 2009a), FGM cylindrical shells (Sofiyev, 2007; Sofiyev and Kuruoglu, 2014), FGM conical shells (Sofiyev, 2009; Sofiyev and Schnack, 2012), and FGM hybrid truncated shells (Sofiyev *et al.*, 2008a,b; Sofiyev, 2019) subjected to mechanical and thermal loads. In their studies, two-parameter elastic foundations were sometimes considered. The effects of foundation, materials and geometric parameters on the buckling pressures and lowest natural frequencies were investigated in detail. Naj *et al.* (2008) employed a first-order shell theory and Sander's nonlinear kinematics equations to study mechanical and thermal buckling behavior of FGM truncated conical shells. They found that the semi-vertex angle, length-to-thickness ratio and radius-to-thickness ratio had significant effects on the buckling mechanical and thermal loads. After investigating dynamic buckling characteristics of imperfect FGM conical shells subjected to an impact load, Zhang and Li (2010) found that the maximal dynamic deflection of an imperfect shell was larger than that of the corresponding perfect shell. By studying buckling behavior of FGM hybrid conical shells reinforced with stiffeners, Dung and Chan (2017) and Duc *et al.* (2018) found that the number of stiffeners could significantly affect the critical loads. The vibration analysis of functionally graded conical and cylindrical shell structures was presented by Tornabene (2009) and Qu *et al.* (2013). The FGMs with a four-parameter power-law distribution was proposed. Vibration characteristics of FGM conical shell panels were investigated by Zhao and Liew (2011). In their study, two types of FGMs, Al/ZrO_2 and Ti-6Al-4V aluminum oxide were taken into account. Using the differential quadrature method (DQM), Heydarpour *et al.* (2014) studied vibration behavior of FGM truncated conical shells subjected to internal pressures. For rotating FGM conical shells, Malekzadeh and Heydarpour (2013) and Dey *et al.* (2015) discussed the effect of rotational speed on natural frequencies. They found that the influence of Coriolis acceleration on the frequency depends

on the shell boundary conditions. Using the variational principle in conjunction with the modified Fourier series, Su *et al.* (2014) obtained an analytical solution of thick FGM conical shells, cylindrical shells and annular plate structures. In addition, vibration of FGM conical shells was studied by Deniz *et al.* (2016) and Zarei *et al.* (2020).

In the above-mentioned studies, the conical shells were treated as perfect structures without pores. However, porosities inevitably appear inside the materials in the process of fabricating FGMs (Wu *et al.*, 2020) and affect Young's moduli (Sofiyev *et al.*, 2009b). Hence, it is necessary to investigate the influence of internal pores on buckling and vibration characteristics of FGM conical shells. Hoa *et al.* (2020) investigated the effects of pores on the critical load of FGM conical shells on elastic foundations. Buckling and vibration characteristics of porous FGM conical shells were also studied by Cuong-Le *et al.* (2021) and Yan *et al.* (2020). All of the results showed that the porosity distributions and porosity volume fraction could affect the statics and dynamics of FGM conical shells. Moreover, the used model for evaluating FGM material properties was based on the model of estimating typical mechanical properties of metal foams, and not the law of mixture.

A sigmoid functionally graded material (S-FGM) is a new kind of composite in which the ceramic volume fraction is described by a sigmoid distribution law. Compared with typical FGMs, S-FGMs have the advantage of eliminating stress concentration in some interfaces where the materials are continuous but quickly varying. Hence, S-FGMs can be used in some engineering structures subjected to impact and thermal loads to avoid concentration of stress. Up to now, few studies have been devoted to buckling and vibration of S-FGM truncated conical shells (Dung *et al.*, 2019; Nemati and Mahmoodabadi, 2020).

As reviewed above, the number of studies on the buckling and vibration of S-FGM conical shells is still rather scarce. According to the authors' knowledge, no previous research work has been done for the buckling and vibration of porous S-FGM shells. Hence, the present study attempts to present a modified model of estimating material properties and investigate the effect of internal pores on the buckling and vibration of porous S-FGM conical shells.

2. A porous S-FGM truncated conical shell

As depicted in Fig. 1, a porous S-FGM truncated conical shell subjected to external pressures P_1 and P_2 is considered. A curvilinear coordinate system (s, θ, z) is set in the middle surface of the cone. s and θ axes lie along the generator and in the circumferential direction. The z axis is perpendicular to the s-θ curve. The radii of the cone at the small and large ends are S_1 and S_2, respectively. L, h and γ denote length, thickness and semi-vertex, respecively. The truncated conical shell is made of ceramic and metal materials. Two types of porosity distributions, even and uneven, are considered (see, Fig. 2).

In the previous open literature, the pore volume fraction α is usually assumed to be very small $\alpha \ll 1$ and neglected in calculating the total volume of porous structures, i.e. $V_c + V_m = 1$, in which V_c and V_m denote the ceramic and metal volume fractions. To eliminate the assumption, we now let $V_c + V_m + \alpha = 1$ and $W_c + W_m = 1$, in which W_c and W_m are the ceramic and metal mass fractions, respectively. Thus, V_c can be calculated as follows

$$V_c = (1 - \alpha)\frac{W_c/\rho_c}{W_c/\rho_c + W_m/\rho_m} \tag{2.1}$$

where ρ_c and ρ_m are the ceramic and metal mass densities.

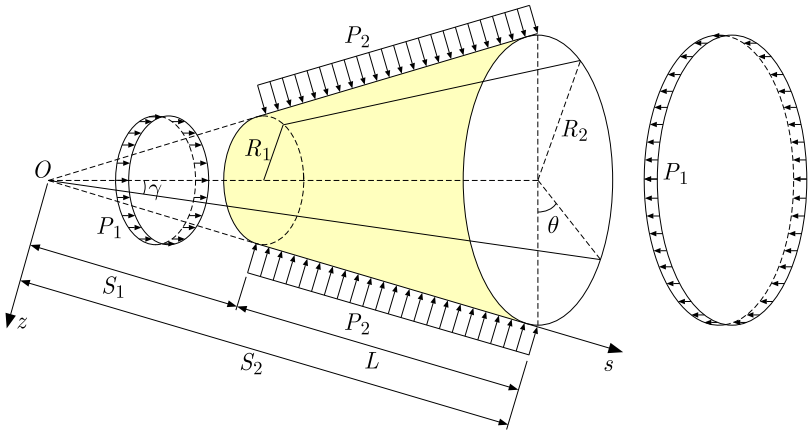

Fig. 1. Scheme of a S-FGM truncated conical shell

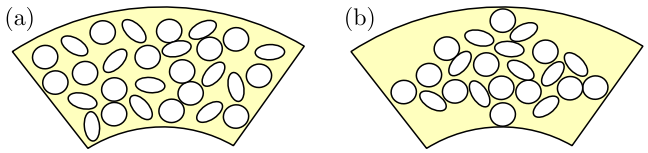

Fig. 2. Porosity distributions: (a) even, (b) uneven

The ceramic volume distribution V_c^* of the S-FGMs is assumed to be

$$V_c^*(z) = \begin{cases} V_{c1}\Big(1 - \dfrac{1}{2}\Big(\dfrac{h/2 - z}{h/2}\Big)^N\Big) & \text{for} \quad 0 \leqslant z \leqslant \dfrac{h}{2} \\ \dfrac{1}{2}V_{c1}\Big(\dfrac{h/2 + z}{h/2}\Big)^N & \text{for} \quad -\dfrac{h}{2} \leqslant z \leqslant 0 \end{cases} \tag{2.2}$$

but V_c^* for typical FGMs is

$$V_c^* = V_{c2}\Big(1 + \frac{2z}{h}\Big)^N \tag{2.3}$$

where N is the material volume index. The coefficients V_{c1} and V_{c2} can be calculated by

$$\int_{-0.5h}^{0.5h} V_c^*(z)\, dz = \int_{-0.5h}^{0.5h} V_c\, dz \tag{2.4}$$

Applying the modified rule of mixture, the effective Young's modulus $E(z)$, mass density $\rho(z)$ and Poisson's ratio $\nu(z)$ of the conical shell can be expressed as follows

$$\begin{aligned} E(z) &= E_c V_c^*(z) + E_m[1 - V_c^*(z) - \alpha^*(z)] \\ \rho(z) &= \rho_c V_c^*(z) + \rho_m[1 - V_c^*(z) - \alpha^*(z)] \\ \nu(z) &= \nu_c V_c^*(z) + \nu_m[1 - V_c^*(z) - \alpha^*(z)] \end{aligned} \tag{2.5}$$

where E_c and ν_c are Young's modulus and Poisson's ratio of the ceramics. E_m and ν_m are the corresponding values of the metals. The porosity volume distributions α^* for the even distribution (ED) is assumed to be

$$\alpha^*(z) = \alpha \tag{2.6}$$

and the uneven distribution (UD) is assumed to be

$$\alpha^*(z) = \alpha_1\Big(1 - \frac{2|z|}{h}\Big) \tag{2.7}$$

Assuming that the total porosity fractions for different distributions are equivalent, the coefficient α_1 can be determined as follows

$$\int_{-0.5h}^{0.5h} \alpha_1\Big(1-\frac{2|z|}{h}\Big)\,dz = \int_{-0.5h}^{0.5h} \alpha\,dz \tag{2.8}$$

3. Formulations

3.1. Governing equations

In the framework of the classical thin shell theory, the stress-strain relationship of the S-FGM conical shell can be expressed as follows

$$\begin{bmatrix}\sigma_s\\ \sigma_\theta\\ \sigma_{s\theta}\end{bmatrix} = \frac{E(z)}{1-\nu^2(z)}\begin{bmatrix}1 & \nu(z) & 0\\ \nu(z) & 1 & 0\\ 0 & 0 & 1-\nu(z)\end{bmatrix}\begin{bmatrix}\varepsilon_s - z\dfrac{\partial^2 W}{\partial s^2}\\ \varepsilon_\theta - z\Big(\dfrac{1}{s^2}\dfrac{\partial^2 W}{\partial \psi^2}+\dfrac{1}{s}\dfrac{\partial W}{\partial s}\Big)\\ \varepsilon_{s\theta} - z\Big(\dfrac{1}{s}\dfrac{\partial^2 W}{\partial s\partial \psi}-\dfrac{1}{s^2}\dfrac{\partial W}{\partial \psi}\Big)\end{bmatrix} \tag{3.1}$$

in which σ_s, σ_θ and $\sigma_{s\theta}$ are the stresses of the middle surface, ε_s, ε_θ and $\varepsilon_{s\theta}$ are the corresponding strains, W is the displacement in the circumferential direction and $\psi = \theta\sin\gamma$.

The membrane forces $(N_s, N_\theta, N_{s\theta})$ and moments $(M_s, M_\theta, M_{s\theta})$ are calculated as

$$[(N_s, N_\theta, N_{s\theta}), (M_s, M_\theta, M_{s\theta})] = \int_{-h/2}^{h/2} [1, z](\sigma_s, \sigma_\theta, \sigma_{s\theta})\,dz \tag{3.2}$$

Introducing stress function $F(s,\psi,t)$, the membrane forces are expressed as

$$(N_s, N_\theta, N_{s\theta}) = \Big(\frac{1}{s^2}\frac{\partial^2 F}{\partial\psi^2}+\frac{1}{s}\frac{\partial\psi}{\partial s}, \frac{\partial^2 F}{\partial s^2}, -\frac{1}{s}\frac{\partial^2 F}{\partial s\partial\psi}+\frac{1}{s^2}\frac{\partial F}{\partial\psi}\Big) \tag{3.3}$$

On the condition that the truncated conical shell is subjected to external pressures P_1 and P_2, the initial membrane forces are given as (Sofiyev, 2009)

$$N_s^0 = -\frac{1}{2}P_1 s\tan\gamma \qquad N_\theta^0 = -P_2 s\tan\gamma \qquad N_{s\theta}^0 = 0 \tag{3.4}$$

Combined with the effects of the initial membrane forces N_s^0, N_θ^0 and $N_{s\theta}^0$, the dynamic equilibrium equations and the strain compatibility equations are built as follows

$$\begin{aligned}&\frac{\partial^2 M_s}{\partial s^2}+\frac{2}{s}\frac{\partial M_s}{\partial s}+\frac{2}{s}\frac{\partial^2 M_{s\theta}}{\partial s\partial\psi}-\frac{1}{s}\frac{\partial M_\theta}{\partial s}+\frac{2}{s^2}\frac{\partial M_{s\theta}}{\partial\psi}+\frac{1}{s^2}\frac{\partial^2 M_\theta}{\partial\psi^2}+\frac{N_\theta}{s}\cot\gamma\\ &\quad+N_s^0\frac{\partial^2 W}{\partial s^2}+\frac{N_\theta^0}{s}\Big(\frac{1}{s}\frac{\partial^2 W}{\partial\psi^2}+\frac{\partial W}{\partial s}\Big)+2N_{s\theta}^0\frac{\partial}{\partial s}\Big(\frac{1}{s}\frac{\partial W}{\partial\psi}\Big)-\rho_t h\frac{\partial^2 W}{\partial t^2}=0\\ &\frac{\cot\gamma}{s}\frac{\partial^2 W}{\partial s^2}-\frac{2}{s}\frac{\partial^2 e_{s\theta}}{\partial s\partial\psi}-\frac{2}{s^2}\frac{\partial e_{s\theta}}{\partial\psi}+\frac{\partial^2 e_\theta}{\partial s^2}+\frac{1}{s^2}\frac{\partial^2 e_s}{\partial\psi^2}+\frac{2}{s}\frac{\partial e_\theta}{\partial s}-\frac{1}{s}\frac{\partial e_s}{\partial s}=0\end{aligned} \tag{3.5}$$

where $\rho_t = \int_{-0.5}^{0.5}\rho(z)\,dz$.

Substituting Eqs. (3.1)-(3.4) into equations (3.5) and introducing the independent variable $x = \ln(s/s_2)$, the governing equations of the S-FGM conical shell can be derived as follows

$$\begin{aligned}&L_1(F)+L_2(W)+P_1L_3(W)+P_2L_4(W)-\rho_t h s_2^4\frac{\partial^2 W}{\partial t^2}=0\\ &L_5(F)+L_6(W)=0\end{aligned} \tag{3.6}$$

where the linear operators L_i $(i=1,\ldots,6)$ are given in Appendix A.

3.2. The solution of the governing equations

In the present study, The free supported boundary conditions are assumed to be

$$s = s_1 \qquad \text{and} \qquad s = s_2 \qquad \Rightarrow \qquad W = M_s = T_s = 0 \tag{3.7}$$

The solution to the governing equations is assumed as

$$\begin{aligned} W &= w(t)\mathrm{e}^{\mu x}\sin(\beta_1 x)\cos(\beta_2\psi) \\ F &= f(t)\mathrm{e}^{(\mu+1)x}\sin(\beta_1 x)\cos(\beta_2\psi) \end{aligned} \tag{3.8}$$

where β_1 and β_2 are the coefficients of the vibration mode (m, n), defined by

$$\beta_1 = \frac{m\pi}{x_0} \qquad \beta_2 = \frac{n}{\sin\gamma} \qquad x_0 = \ln\frac{s_2}{s_1} \tag{3.9}$$

The parameter μ is introduced to obtain the minimum values of the critical pressure and lowest frequency. Multiplying Eq. $(3.6)_1$ by $s_2^2\exp[(\mu+2)x]\sin(\beta_1 x)\cos(\beta_2\psi)$ and $(3.6)_2$ by $s_2^3\exp[(\mu+3)x]\sin(\beta_1 x)\cos(\beta_2\psi)$, then applying Galerkin's method over the shell area $0 \leqslant \psi \leqslant 2\pi\sin\gamma$ and $-x_0 \leqslant x \leqslant 0$, the following differential equation with respect to time t can be derived

$$\frac{\partial^2 w}{\partial t^2} + \frac{1}{G_7}\Big(-\frac{G_1 G_6}{G_5} + G_2 + P_1 G_3 + P_2 G_4\Big)w(t) = 0 \tag{3.10}$$

where the coefficients G_i $(i = 1, \ldots, 7)$ are defined by

$$\begin{aligned} G_1 &= \frac{1}{G_4}\int_{-x_0}^{0}\int_{0}^{2\pi\sin\gamma} L_1(F)s_2^2\mathrm{e}^{(\mu+2)x}\sin(\beta_1 x)\cos(\beta_2\psi)\,dx\,d\psi \\ G_2 &= \int_{-x_0}^{0}\int_{0}^{2\pi\sin\gamma} L_2(W)s_2^2\mathrm{e}^{(\mu+2)x}\sin(\beta_1 x)\cos(\beta_2\psi)\,dx\,d\psi \\ G_3 &= \int_{-x_0}^{0}\int_{0}^{2\pi\sin\gamma} L_3(W)s_2^2\mathrm{e}^{(\mu+2)x}\sin(\beta_1 x)\cos(\beta_2\psi)\,dx\,d\psi \\ G_4 &= \int_{-x_0}^{0}\int_{0}^{2\pi\sin\gamma} L_4(W)s_2^2\mathrm{e}^{(\mu+2)x}\sin(\beta_1 x)\cos(\beta_2\psi)\,dx\,d\psi \\ G_5 &= \int_{-x_0}^{0}\int_{0}^{2\pi\sin\gamma} L_5(F)s_2^3\mathrm{e}^{(\mu+3)x}\sin(\beta_1 x)\cos(\beta_2\psi)\,dx\,d\psi \\ G_6 &= \int_{-x_0}^{0}\int_{0}^{2\pi\sin\gamma} L_6(W)s_2^3\mathrm{e}^{(\mu+3)x}\sin(\beta_1 x)\cos(\beta_2\psi)\,dx\,d\psi \\ G_7 &= -\int_{-x_0}^{0}\int_{0}^{2\pi\sin\gamma} \rho_f h s_2^6\frac{\partial^2 W}{\partial t^2}\mathrm{e}^{(\mu+2)x}\sin(\beta_1 x)\cos(\beta_2\psi)\,dx\,d\psi \end{aligned} \tag{3.11}$$

If the conical shell is free from external pressures $P_1 = P_2 = 0$, the frequency ω of the free vibration is obtained as

$$\omega = \sqrt{\frac{1}{G_7}\Big(-\frac{G_1 G_6}{G_5} + G_2\Big)} \tag{3.12}$$

According to equation (3.10), the critical hydraulic buckling pressures $P_1 = P_2 = P_{Hcr}$ and lateral buckling pressures $P_1 = 0$, $P_2 = P_{L\,cr}$ are obtained as

$$P_{H\,cr} = -\frac{G_1G_6 - G_2G_5}{G_5(G_3 + G_4)} \qquad P_{L\,cr} = -\frac{G_1G_6 - G_2G_5}{G_5G_4} \tag{3.13}$$

It is noted that the minimum values of buckling pressure and frequency obtained by Eqs. (3.12) and (3.13) depend on the parameters m, n and μ. In the present study, the minimum value of the shape mode (m, n) can be found by changing the value of the parameter μ from 0 to 5 with the step 0.1 (Sofiyev, 2009).

4. Results and discussion

4.1. Comparison studies

To validate the present method, two numerical examples are tested and the results are listed in Tables 1 and 2.

Example 1. The buckling behavior of a typical FGM truncated conical shell is studied in this example. The critical loads $P_{H\,cr}$ and $P_{L\,cr}$ are displayed in Table 1. The materials properties for silicon nitride (Si_3N_4) are $E_c = 0.32227\,\text{TPa}$, $\rho_c = 2370\,\text{kg/m}^3$ and $\nu_c = 0.24$. Those for stainless steel (SUS304) are $E_m = 0.2077877\,\text{TPa}$, $\rho_m = 8166\,\text{kg/m}^3$ and $\nu_m = 0.317756$. The geometric parameters are $R_1 = 1.0\,\text{m}$, $R_2 = 3.0\,\text{m}$, $R_2/h = 200$ and $\gamma = 30^\circ$. It can be observed that the present results agree well with those given by Sofiyev (2009). The maximum error is only 0.5%.

Table 1. Comparison of the critical pressures $P_{H\,cr}$ and $P_{L\,cr}$ for a typical FGM truncated conical shell

N	Method	$P_{H\,cr}(n,\mu)$ [MPa]	$P_{L\,cr}(n,\mu)$ [MPa]
Si_3N_4 ($N = 0$)	Sofiyev (2009)	0.741(8,2.1)	0.779(8,1.9)
	Present	0.739(8,2.1)	0.776(8,1.9)
	Discrepancy	0.3%	0.4%
1.0	Sofiyev (2009)	0.578(8,2.1)	0.607(8,1.9)
	Present	0.575(8,2.1)	0.604(8,1.9)
	Disfrepancy	0.5%	0.5%
2.0	Sofiyev (2009)	0.551(8,2.1)	0.579(8,1.9)
	Present	0.548(8,2.1)	0.577(8,1.9)
	Discrepancy	0.5%	0.3%

Example 2. The free vibration of a typical FGM truncated conical is studied in the example. The materials properties for silicon nitride (Si_3N_4) are $E_c = 0.32227\,\text{TPa}$, $\rho_c = 2370\,\text{kg/m}^3$ and $\nu_c = 0.24$, and the those for Nicknel (Ni) are $E_m = 0.205098\,\text{TPa}$, $\rho_m = 8900\,\text{kg/m}^3$ and $\nu_m = 0.31$. The geometric parameters of the shell are $R_2/h = 100$, $L = 2R_1$ and $\gamma = 30^\circ$. The dimensionless fundamental frequency $\Omega_1 = \omega_1 R_2\sqrt{(1-\nu_c^2)\rho_c/E_c}$ is calculated and listed in Table 2. It can be seen that the maximum deviation between the present results and those given by Sofiyev and Schnack (2012) is 0.6%.

4.2. Parametric studies

After the present method is validated, the effects of the porosity volume fraction, porosity distribution, material volume index, semi-vertex angle on the critical buckling loads and the

Table 2. Comparison of the dimensionless fundamental frequency Ω_1 for a typical FGM truncated conical shell

Method	N_i	$N = 1.0$	$N = 2.0$	Si_3N_4
Sofiyev and Schnack (2012)	0.0723(7)	0.0997(7)	0.0887(7)	0.1763(7)
Present	0.0725(7,1.1)	0.1002(7,1.0)	0.0892(7,1.1)	0.1757(7,1.1)
Discrepancy	0.3%	0.5%	0.6%	0.4%

lowest natural frequencies of porous S-FGM truncated conical shells are discussed in this Subsection. The material and geometric parameters are given in Example 1. Unless specially stated, the following parameters are used: $W_c = 0.3$, $\alpha = 0.1$ and $N = 1.0$.

Tables 3 and 4 list the first five buckling pressures $P_{H\,cr}$, $P_{L\,cr}$ and natural frequency ω of the porous conical shell. The two kinds of pore distributions, even distribution (ED) and uneven distribution (UD) are taken into account. It can be found that the minimum values of the buckling pressures are obtained in mode (1,7). However, the lowest frequency is obtained in mode (1,5). Also, it can be observed that the parameter μ for the critical buckling pressures is about 2.7, but that for the lowest frequency it is 1.1. Moreover, it can be found that the minimum values of the buckling pressures $P_{H\,cr}$, $P_{L\,cr}$ and frequency ω for the even distribution are smaller than the corresponding values for the uneven distribution, respectively. It can be proved that the effective rigidity for the even distribution is larger than that for the uneven one.

Table 3. Buckling pressures $P_{H\,cr}$, $P_{L\,cr}$ and frequency ω of different modes (m, n) for a porous S-FGM truncated conical shell with evenly distributed pores

(m, n)	(1,7)	(1,6)	(1,8)	(1,5)	(2,8)
$P_{H\,cr}(\mu)$ [MPa]	0.442(2.7)	0.447(1.7)	0.462(3.8)	0.542(0.8)	0.574(3.0)
$P_{L\,cr}(\mu)$ [MPa]	0.461(2.6)	0.465(1.6)	0.485(3.6)	0.567(0.8)	0.624(2.7)
(m, n)	(1,5)	(1,6)	(1,4)	(1,7)	(1,8)
$\omega(\mu)$ [Hz]	51.791(1.1)	54.699(1.9)	59.401(0.5)	61.732(3.0)	70.702(4.0)

Table 4. Buckling pressures $P_{H\,cr}$, $P_{L\,cr}$ and frequency ω of different modes (m, n) for a porous S-FGM truncated conical shell with unevenly distributed pores

(m, n)	(1,7)	(1,6)	(1,8)	(1,5)	(2,8)
$P_{H\,cr}(\mu)$ [MPa]	0.460(2.6)	0.462(1.7)	0.482(3.7)	0.557(0.8)	0.594(3.1)
$P_{L\,cr}(\mu)$ [MPa]	0.481(2.7)	0.484(1.7)	0.507(3.7)	0.582(0.8)	0.645(2.7)
(m, n)	(1,5)	(1,6)	(1,4)	(1,7)	(1,8)
$\omega(\mu)$ [Hz]	52.461(1.1)	55.685(2.0)	59.706(0.5)	62.986(3.0)	72.231(4.1)

For the sake of revealing the effect of the parameter μ on the buckling and vibration behavior of the truncated conical shell, the curves of the buckling pressure $P_{H\,cr}$ and $P_{L\,cr}$ versus the parameter μ are displayed in Fig. 3a. As the parameter μ changes from 0.0 to 2.7, the buckling pressures $P_{H\,cr}$ and $P_{L\,cr}$ decrease. However, the buckling pressures increase as the parameter changes from 2.7 to 5.0. Thus, it can be found that the critical buckling pressures can be obtained at $\mu \approx 2.7$. A similar variation of the natural frequency versus the parameter μ is observed in Fig. 3b, but the lowest frequency ω can be obtained at $\mu \approx 1.1$.

The curves of the buckling pressures $P_{H\,cr}$, $P_{L\,cr}$ and lowest frequency ω versus the ceramic mass fraction W_c are shown in Figs. 4a and 4b. From the two figures, it can be observed that the values of $P_{H\,cr}$, $P_{L\,cr}$ and ω are increased with an increase in W_c. It is due to the fact that Young's modulus of Si_3N_4 is higher than that of Ni. Also, it can be seen that the critical buckling

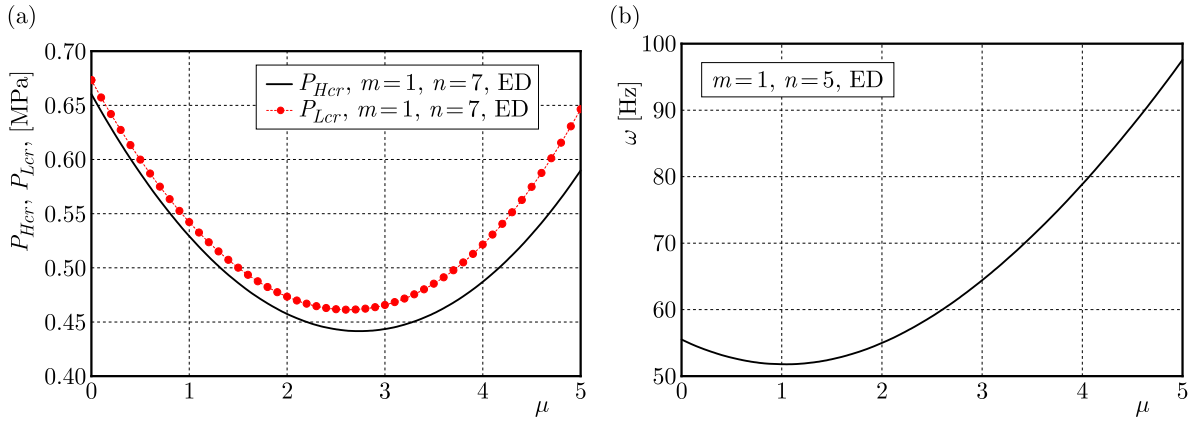

Fig. 3. Effect of the parameter on: (a) critical buckling pressures, (b) lowest frequency

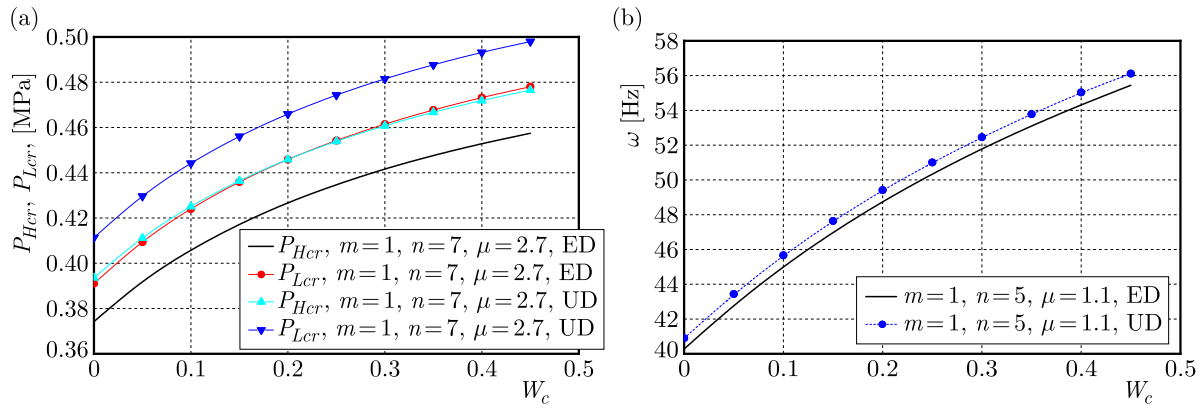

Fig. 4. Effect of the ceramic mass fraction W_C on: (a) buckling pressures $P_{H\,cr}$ and $P_{L\,cr}$, (b) lowest frequency ω

pressure $P_{H\,cr}$ for the even distribution is very close to the critical lateral pressure $P_{L\,cr}$ for the uneven distribution. The lowest frequency for the uneven distribution is higher than that for the even porosity distribution. Also, this demonstrates that the effective rigidity of the former is larger than that of the latter.

In Fig. 5a, the influence of the porosity volume fraction α on the buckling pressures $P_{H\,cr}$ and $P_{L\,cr}$ is revealed. It is clear that the values of $P_{H\,cr}$ and $P_{L\,cr}$ decreased with an increasing value of α. The decrease in the buckling hydraulic pressure $P_{H\,cr}$ is more significant than that of the buckling lateral pressure $P_{L\,cr}$. If the value of α varies from 0 to 0.3, the value of $P_{H\,cr}$ for the uneven and even distribution decreases by about 21% and 32%, respectively. It is evident that the effect of the porosity volume fraction on the buckling hydraulic pressure for the even porosity distribution is more significant than that for uneven porosity distribution.

The variation curves of the lowest frequency ω versus porosity volume fraction α are shown in Fig. 5b. It can be observed that the variation is different for different porosity distributions. The lowest frequency ω for the even distribution is decreased by increasing α. On the contrary, the lowest frequency ω for the uneven distribution is increased as α increases. Also, one can notice the turning point of the variation curves for the uneven distribution at $\alpha = 0.24$. Furthermore, the value of ω for $\alpha > 0.4$ increases more slowly than that for $\alpha < 0.24$.

The effects of the material index N on the buckling pressures $P_{H\,cr}$ and $P_{L\,cr}$ are shown in Fig. 6a. It is clear that the values of buckling pressures are decreased with an increase of the index N. This is because the increase of N indicates a decrease in the volume fraction of Si_3N_4, which leads to a decrease in the shell effective rigidity. As expected, the curve of buckling

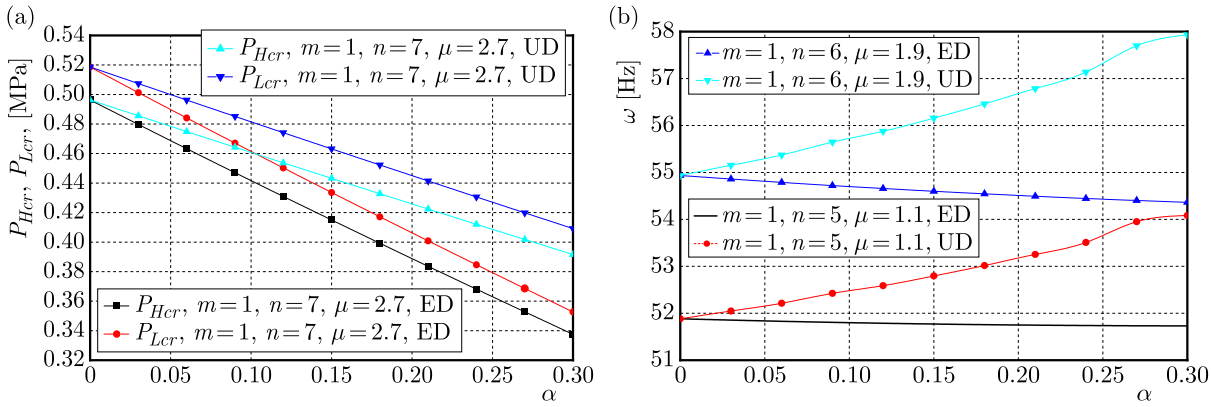

Fig. 5. Effect of the pore volume fraction α on: (a) buckling pressures $P_{H\,cr}$ and $P_{L\,cr}$, (b) lowest frequency ω

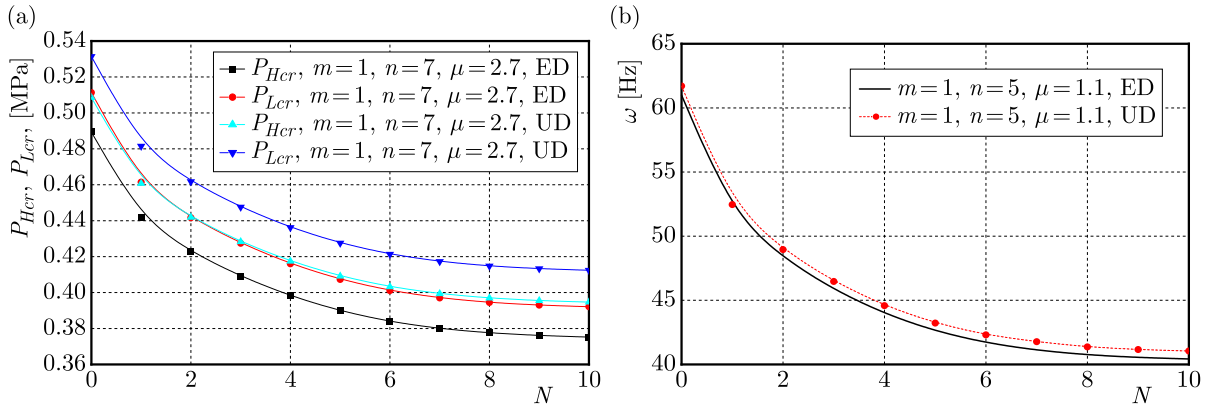

Fig. 6. Effect of the material index N on: (a) buckling pressures $P_{H\,cr}$ and $P_{L\,cr}$, (b) lowest frequency ω

hydraulic pressure $P_{H\,cr}$ for the uneven distribution is very close to the curve of buckling lateral pressure $P_{L\,cr}$ for the even distribution. This proves that the effective rigidity of the former nearly equals that of the latter. Figure 6b shows the effect of the material index N on the lowest frequency ω. It is seen that the value of ω can be decreased by increasing the index N. This is due to the fact that an increase in N leads to a decrease in the effective rigidity of the truncated conical shell.

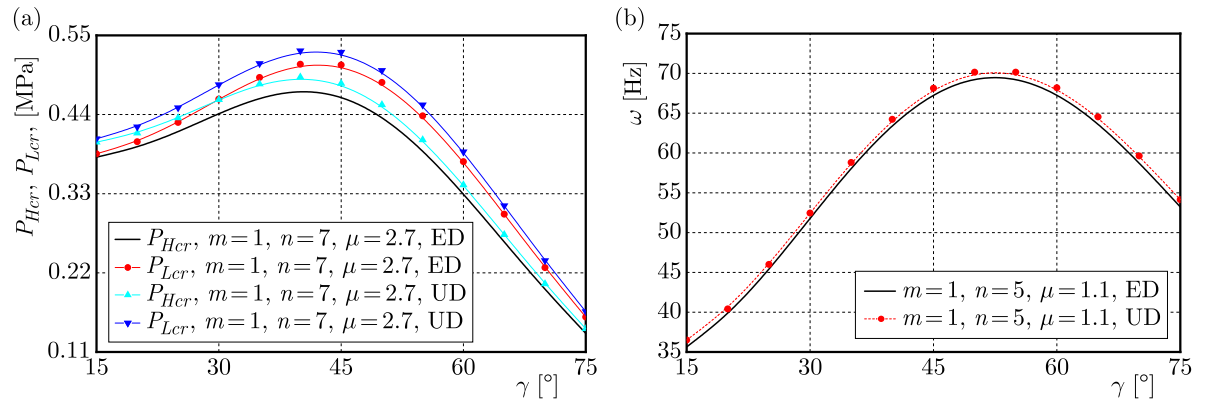

Fig. 7. Effect of the semi-vertex angle γ on: (a) buckling pressures $P_{H\,cr}$ and $P_{L\,cr}$, (b) lowest frequency ω

The curves of the buckling pressures $P_{H\,cr}$ and $P_{L\,cr}$ versus semi-vertex angle γ are shown in Fig. 7a. From the figure, it can be seen that the maximum values of buckling pressures $P_{H\,cr}$, $P_{L\,cr}$ and frequency ω are obtained at $\gamma \approx 40°$, which implies that the maximum of the shell effective rigidity is obtained at $\gamma \approx 40°$. The variation of the lowest frequency ω varying with the semi-vertex angle γ are shown in Fig. 7b. It can be observed that the maximum value of the lowest frequency ω is reached at $\gamma \approx 50°$. Also, it can be observed that the porosity distribution has an insignificant effect on the lowest frequency. The maximum difference is about 2.4%.

5. Conclusion

This paper presents a new reliable model to evaluate material properties of sigmoid functionally graded materials. The buckling and vibration of porous S-FGM truncated conical shells are investigated. The present results are compared with those available in the open literature. In the parametric studies, the effects of ceramic mass fraction, porosity volume fraction, porosity distribution, material index and semi-vertex angle are discussed in detail. The results show that both the porosity volume fraction and distribution have significant effects on the buckling pressures and lowest frequency. The buckling pressures and lowest frequency for the even porosity distribution are decreased as the porosity volume fraction rises. However, the lowest frequency for the uneven porosity distribution is increased. By increasing the ceramic mass fraction, the values of buckling pressures and lowest frequency can be raised. As the semi-vertex angle γ changes from 15° to 75°, the critical buckling pressure and lowest frequency are obtained at about 40° and 50°, respectively.

A. Appendix

$$
\begin{aligned}
L_1(F) &= A_1\mathrm{e}^{-4x}\Big(\frac{\partial^4 F}{\partial x^4} - 4\frac{\partial^3 F}{\partial x^3} + 4\frac{\partial^2 F}{\partial x^2} + 2\frac{\partial^2 F}{\partial \psi^2} + \frac{\partial^4 F}{\partial \psi^4}\Big)\\
&\quad - s_2\mathrm{e}^{-3x}\cot\gamma\frac{\partial F}{\partial x} + s_2\mathrm{e}^{-3x}\cot\gamma\frac{\partial^2 F}{\partial x^2} + A_2\mathrm{e}^{-4x}\Big(\frac{\partial^4 F}{\partial x^2\partial \psi^2} - 2\frac{\partial^3 F}{\partial x\partial \psi^2} + \frac{\partial^2 F}{\partial \psi^2}\Big)\\
L_2(W) &= -A_3\mathrm{e}^{-4x}\Big(\frac{\partial^4 W}{\partial x^4} - 4\frac{\partial^3 W}{\partial x^3} + 4\frac{\partial^2 W}{\partial x^2} + 2\frac{\partial^2 W}{\partial \psi^2} + \frac{\partial^4 W}{\partial \psi^4}\Big)\\
&\quad - A_4\mathrm{e}^{-4x}\Big(\frac{\partial^4 W}{\partial x^2\partial \psi^2} - 2\frac{\partial^3 W}{\partial x\partial \psi^2} + \frac{\partial^2 W}{\partial \psi^2}\Big)\\
L_3(W) &= \frac{1}{2}s_2^3\mathrm{e}^{-x}\tan\gamma\Big(\frac{\partial W}{\partial x} - \frac{\partial^2 W}{\partial x^2}\Big) \qquad L_4W = -s_2^3\mathrm{e}^{-x}\tan\gamma\Big(\frac{\partial W}{\partial x} + \frac{\partial^2 W}{\partial \psi^2}\Big)\\
L_5(F) &= B_1\mathrm{e}^{-4x}\Big(\frac{\partial^4 F}{\partial x^4} - 4\frac{\partial^3 F}{\partial x^3} + 4\frac{\partial^2 F}{\partial x^2} + 2\frac{\partial^2 F}{\partial \psi^2} + \frac{\partial^4 F}{\partial \psi^4}\Big)\\
&\quad + B_2\mathrm{e}^{-4x}\Big(\frac{\partial^4 F}{\partial x^2\partial \psi^2} - 2\frac{\partial^3 F}{\partial x\partial \psi^2} + \frac{\partial^2 F}{\partial \psi^2}\Big)\\
L_6(W) &= -B_3\mathrm{e}^{-4x}\Big(\frac{\partial^4 W}{\partial x^4} - 4\frac{\partial^3 W}{\partial x^3} + 4\frac{\partial^2 W}{\partial x^2} + 2\frac{\partial^2 W}{\partial \psi^2} + \frac{\partial^4 W}{\partial \psi^4}\Big)\\
&\quad + B_4\mathrm{e}^{-4x}\Big(\frac{\partial^4 W}{\partial x^2\partial \psi^2} - 2\frac{\partial^3 W}{\partial x\partial \psi^2} + \frac{\partial^2 W}{\partial \psi^2}\Big) + s_2\mathrm{e}^{-3x}\cot\gamma\Big(\frac{\partial^2 W}{\partial x^2} - \frac{\partial W}{\partial x}\Big)
\end{aligned}
\tag{A.1}
$$

In which coefficients A_i and B_i are defined by

$$
\begin{aligned}
&A_1 = c_{12} \qquad A_2 = 2(c_{11} - c_{31}) \qquad A_3 = c_{13} \qquad A_4 = 2(c_{14} + c_{32})\\
&B_1 = b_{11} \qquad B_2 = 2(b_{31} + b_{12}) \qquad B_3 = b_{14} \qquad B_4 = 2(b_{32} - b_{13})
\end{aligned}
$$

$$c_{11} = a_{11}^1 b_{11} + a_{12}^1 b_{12} \qquad c_{12} = a_{11}^2 b_{12} + a_{12}^1 b_{12} \qquad c_{13} = a_{11}^1 b_{13} + a_{12}^1 b_{14} + a_{11}^2$$
$$c_{14} = a_{11}^1 b_{14} + a_{12}^1 b_{13} + a_{12}^2 \qquad c_{31} = a_{66}^1 b_{31} \qquad c_{32} = a_{66}^1 b_{32} + a_{66}^2 \tag{A.2}$$

$$b_{11} = a_{11}^0 d_0 \qquad b_{12} = -a_{12}^0 d_0 \qquad b_{13} = (a_{12}^0 a_{12}^1 - a_{11}^1 a_{11}^0) d_0$$
$$b_{14} = (a_{12}^0 a_{11}^1 - a_{12}^1 a_{11}^0) d_0 \qquad b_{31} = \frac{1}{a_{66}^0} \qquad b_{32} = -\frac{a_{66}^1}{a_{66}^0}$$
$$d_0 = \frac{1}{a_{11}^0 a_{11}^0 - a_{12}^0 a_{12}^0}$$

In Eqs. (A.2), the coefficients a_{ij}^k are defined as follows

$$a_{11}^k = \int_{-0.5h}^{0.5h} z^k \frac{E(z)}{1-\nu^2(z)}\, dz \qquad a_{12}^k = \int_{-0.5h}^{0.5h} z^k \frac{\nu(z)E(z)}{1-\nu^2(z)}\, dz$$
$$a_{66}^k = \int_{-0.5h}^{0.5h} z^k \frac{E(z)}{2[1+\nu(z)]}\, dz \tag{A.3}$$

Acknowledgment

The authors are grateful for the financial support of the National Natural Science Foundation of China (No. 12162010) and the Natural Science Foundation of Guangxi (No. 2021GXNSFAA220087).

References

1. Alizada A.N., Sofiyev A.H., 2011, Modified Young's moduli of nano-materials taking into account the scale effects and vacancies, *Meccanica*, **46**, 915-920
2. Chi S.H., Chung Y.L., 2002, Cracking in sigmoid functionally graded coating, *Journal of Mechanics*, **18**, 41–53
3. Cuong-Le T., Nguyen K.N., Nguyen-Trong N., Khatir S., Nguyen-Xuan H., Abdel--Wahab M., 2021, A three-dimensional solution for free vibration and buckling of annular plate, conical, cylinder and cylindrical shell of FG porous-cellular materials using IGA, *Composite Structures*, **259**, 113216
4. Deniz A., Zerin Z., Karaca Z., 2016, Winkler-Pasternak foundation effect on the frequency parameter of FGM truncated conical shells in the framework of shear deformation theory, *Composites: Part B*, **104**, 57-70
5. Dey S., Sarkar S., Das A., Karmakar A., Adhikari S., 2015, Effect of twist and rotation on vibration of functionally graded conical shells, *International of Journal of Mechanics and Material Design*, **11**, 425-437
6. Duc N.D., Kim S.E., Chan D.Q., 2018, Thermal buckling analysis of FGM sandwich truncated conical shells reinforced by FGM stiffeners resting on elastic foundations using FSDT, *Journal of Thermal Stresses*, **41**, 3, 331-365
7. Dung D.V., Chan D.Q., 2017, Analytical investigation on mechanical buckling of FGM truncated conical shells reinforced by orthogonal stiffeners based on FSDT, *Composite Structures*, **159**, 827-841
8. Dung D.V., Nga N.T., Vuong P.M., 2019, Nonlinear stability analysis of stiffened functionally graded material sandwich cylindrical shells with general Sigmoid law and power law in thermal environment using third-order shear deformation theory, *Journal of Sandwich Structures and Materials*, **21**, 3, 938-972

9. Heydarpour Y., Malekzadeh P., Aghdam M.M., 2014, Free vibration of functionally graded truncated conical shells under internal pressure, *Meccanica*, **49**, 267-282
10. Hoa L.K., Phi B.G., Chan D., Dang V.D., 2020, Buckling analysis of FG porous truncated conical shells resting on elastic foundations in the framework of the shear deformation theory, *Advances in Applied Mathematics and Mechanics*, **14**, 1, 218-247
11. Malekzadeh P., Heydarpour Y., 2013, Free vibration analysis of rotating functionally graded truncated conical shells, *Composite Structures*, **97**, 176-188
12. Naj R., Boroujerdy M.S., Eslami M.R., 2008, Thermal and mechanical instability of functionally graded truncated conical shells, *Thin-Walled Structures*, **46**, 65-78
13. Nemati A.R., Mahmoodabadi M.J., 2020, Effect of micromechanical models on stability of functionally graded conical panels resting on Winkler-Pasternak foundation in various thermal environments, *Archives of Applied Mechanics*, **90**, 5, 883-915
14. Qu Y.G., Long X.H., Yuan G.Q., Meng G., 2013, A unified formulation for vibration analysis of functionally graded shells of revolution with arbitrary boundary conditions, *Composites: Part B*, **50**, 381-402
15. Sofiyev A.H., 2007, Vibration and stability of composite cylindrical shells containing a FG layer subjected to various loads, *Structural Engineering and Mechanics*, **27**, 365-391
16. Sofiyev A.H., 2009, The vibration and stability behavior of freely supported FGM conical shells subjected to external pressure, *Composite Structures*, **89**, 356-366
17. Sofiyev A.H., 2019, Review of research on the vibration and buckling of the FGM conical shells, *Composite Structures*, **211**, 301-317
18. Sofiyev A.H., Aksogan O., Schnack E., Avcar M., 2008a, The stability of a three-layered composite conical shell containing a FGM layer subjected to external pressure, *Mechanics of Advanced Materials and Structures*, **15**, 461-466
19. Sofiyev A.H., Korkmaz K.A., Mammadov Z., Karmanli M., 2009a, The vibration and buckling of freely supported non-homogeneous orthotropic conical shells subjected to different uniform pressures, *International Journal of Pressure Vessels and Piping*, **86**, 661-668
20. Sofiyev A.H., Kuruoglu N., 2014, Buckling and vibration of shear deformable functionally graded orthotropic cylindrical shells under external pressures, *Thin-Walled Structures*, **78**, 121-130
21. Sofiyev A.H., Kuruoglu N., Turkmen M., 2009b, Buckling of FGM hybrid truncated conical shells subjected to hydrostatic pressure, *Thin-Walled Structures*, **47**, 61-72
22. Sofiyev A.H., Schnack E., 2012, The vibration analysis of FGM truncated conical shells resting on two-parameter elastic foundations, *Mechanics of Advanced Materials and Structures*, **19**, 241-249
23. Sofiyev A.H., Zerin Z., Korkmaz A., 2008b, The stability of a thin three-layered composite truncated conical shell containing a FGM layer subjected to non-uniform lateral pressure, *Composite Structures*, **85**, 105-115
24. Su Z., Jin G.Y., Shi S.G., Ye T.G., Jia X.T., 2014, A unified solution for vibration analysis of functionally graded cylindrical, conical shells and annular plates with general boundary conditions, *International Journal of Mechanical Sciences*, **80**, 62-80
25. Torabi J., Ansari R., 2018, A higher-order isoparametric superelement for free vibration analysis of functionally graded shells of revolution, *Thin-Walled Structures*, **133**, 169-179
26. Tornabene F., 2009, Free vibration analysis of functionally graded conical, cylindrical shell and annular plate structures with a four-parameter power-law distribution, *Computer Methods of Applied Mechanics and Engineering*, **198**, 2911-2935
27. Wu H., Yang J., Kitipornchal S., 2020, Mechanical analysis of functionally graded porous structures: a review, *International Journal of Structural Stability and Dynamics*, **20**, 2041015
28. Yan K., Zhang Y., Cai H., Tahouneh V., 2020, Vibrational characteristic of FG porous conical shells using Donnell's shell theory, *Steel and Composite Structures*, **35**, 2, 249-260

29. Zarei M., Rahimi G.H., Hemmatnezhad M., 2020, Free vibrational characteristics of grid-stiffened truncated composite conical shells, *Aerospace Science and Technology*, **99**, 105717

30. Zhang J.H., Li S.R., 2010, Dynamic buckling of FGM truncated conical shells subjected to non-uniform normal impact load, *Composite Structures*, **92**, 2979-2983

31. Zhao X., Liew K.M., 2011, Free vibration analysis of functionally graded conical shell panels by a meshless method, *Composite Structures*, **93**, 649-664

Manuscript received February 19, 2023; accepted for print May 31, 2023